Triboelectric Nanogenerator Powered Electrowetting-on-Dielectric Actuator for Concealed Aquatic Microbots

Article *in* ACS Nano · November 2020

DOI: 10.1021/acsnano.0c05901

CITATIONS
9

READS
137

7 authors, including:

Dongyue Jiang
Dalian University of Technology
35 PUBLICATIONS **873** CITATIONS
SEE PROFILE

Zeng Fan
National University of Singapore
51 PUBLICATIONS **1,969** CITATIONS
SEE PROFILE

Hongchen Wang
Dalian University of Technology
5 PUBLICATIONS **17** CITATIONS
SEE PROFILE

Minyi Xu
Dalian Maritime University
100 PUBLICATIONS **1,372** CITATIONS
SEE PROFILE

ACS NANO

www.acsnano.org

ARTICLE

Triboelectric Nanogenerator Powered Electrowetting-on-Dielectric Actuator for Concealed Aquatic Microbots

Dongyue Jiang,* Zeng Fan, Hongchen Wang, Minyi Xu,* Guijun Chen, Yongchen Song, and Zhong Lin Wang*

Cite This: *ACS Nano* 2020, 14, 15394−15402

Read Online

ACCESS | Metrics & More | Article Recommendations | Supporting Information

ABSTRACT: **Aquatic microbots have drawn great research interest due to the demands in aquatic environmental monitoring, inspection, and confined space exploration. Current actuation methods heavily rely on mechanical motion powered by large-amplitude and high-frequency sources, which limit the applications with portability and concealment requirements. Herein we propose a triboelectric nanogenerator (TENG)-enabled electrowetting-on-dielectric (EWOD) actuator (TENG-EWA) for aquatic microbots. The transferred tribocharges of a disc TENG alternatively modify the surface energy of the EWOD actuator, yielding a capillary wave propagation. The reaction force of the capillary wave actuates the microbot on the water surface. The characteristics of the TENG induced capillary wave are analyzed experimentally and modeled theoretically. An optical transparent microbot (weight of 0.07 g, body length of 1 cm) was actuated forward at a maximum locomotion velocity of 1 cm/s. Diverse locomotion functions are demonstrated: with a load of 3 times to the robot net weight, in seawater, at a silicone-oil/deionized water interface. Besides, the locomotion of the microbot was demonstrated by a wind-driven TENG, and a good concealment performance was achieved under infrared camera and decibel meter. The proposed aquatic TENG-Bot not only shows the potential of converting environmental energy into actuation force for microbots but also reveals advantages in optical, sonic, and infrared concealment.**

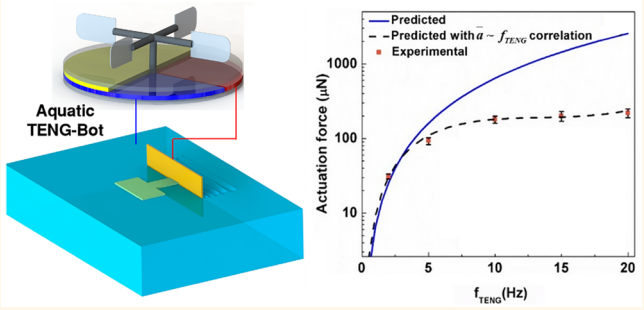

KEYWORDS: *triboelectric nanogenerator, two-phase flow, capillary wave, EWOD, self-powered actuator, aquatic robot*

Aquatic microbots draw increasing attention due to their potential in the applications of water environment monitoring,[1] inspection,[2] and exploration of confined spaces.[3] The actuation of the aquatic microrobots is of great importance since it not only determines the locomotion performance but also poses challenges to the power supply system. Piezoelectric,[4] dielectric elastomer,[5] hydrogel,[6] and DC motors[7] are typically employed by aquatic microrobots to achieve swimming motion on the water surface. However, these actuators face two common challenges. The first challenge originates from the requirement of a large-amplitude and high-frequency power source. The typical working voltage for these actuators ranges from several hundreds to thousands of volts and frequency up to several kilohertz. The usage of the specific high-voltage and high-frequency electric power sources not only increases the investment but also limits the applicability in portable and wild environments. A self-powered or ambient environmental energy powered aquatic microrobot is highly desired. Another challenge of the current actuators is the complex electronics on the microbot including batteries, controls, logics, flaps,[8] legs,[9] or tails to achieve a coordinated swimming motion. Even though these electronics have been significantly optimized, the size of the reported microbots[3,8−11] is still up to ∼1 cm in length and ∼0.1 g in weight. A larger-sized microbot is easier to be detected optically when concealment is taken into consideration by the applications. Furthermore, the mechanical motion of the current actuators induces heat and noise generation, which is also undesirable for sonic and infrared concealment. A lightweight and simple

Received: July 15, 2020
Accepted: November 9, 2020
Published: November 12, 2020

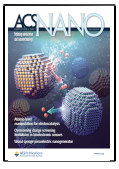

https://dx.doi.org/10.1021/acsnano.0c05901
ACS Nano 2020, 14, 15394−15402

structured actuation mode is favorable for the concealed operation of the aquatic microbots.

Considering the challenges of the current actuators for aquatic microbots, here we present a triboelectric nanogenerator powered EWOD (electrowetting on dielectrics) actuator (TENG-EWA) for aquatic microbots: the aquatic TENG-Bot. The TENG[12−14] developed by Wang's group has shown great potential in ambient mechanical energy harvesting. The TENG converts mechanical stimuli into electricity by contact electrification and electrostatic induction processes.[15,16] These two processes could be simply achieved by touching, pressing, sliding, rotating, and vibrating motions between a couple of materials with opposite surface charges. The optimization of TENG technology has risen[17−19] in recent years, and diverse environmental energy sources including wind, water waves, raindrops, flow streams, and tides have been demonstrated to power small electronics.[20,21] These features make the TENG a good candidate to convert environmental energy for powering aquatic microbots. On the other hand, an AC EWOD-based capillary propulsion technology proposed by Cho *et al.*[22,23] has shown great potential in floating object actuation. The AC EWOD-based capillary propulsion possesses superior performances including moving parts free and simple device configuration. These features are favorable in pursuing a concealed aquatic microbot.

As an emerging power source, the TENG is widely employed for powering small electronics as self-powered sensors. However, the application of using TENGs for the actuation of aquatic microbots has not been well studied or exploited. This study investigates the detailed working characteristics of a TENG when actuating an aquatic microbot (*e.g.*, open-circuit voltage and frequency of the TENG, electrode width of actuator, and ions in the aqueous solution). Further, a theoretical model is established in this work for predicting the relationship between the TENG output signal and the actuation force of the microbot. Due to the simple device configuration, an ultralightweight tethered aquatic TENG-Bot of 0.07 g (1 cm in length, 2 cm in width, and 0.8 cm in height) is assembled by an optically transparent PET (polyethylene terephthalate) robot frame and demonstrated moving forward at a maximum locomotion speed of 1 cm/s by the TENG. As compared to the conventional actuator-enabled aquatic microbots, the proposed aquatic TENG-Bot provides the following advantages: (i) the actuation is achieved by a TENG device that converts environmental energy into actuation force, thus relieving the dependence on high-voltage, high-frequency power sources and improving the applicability in a portable and wild environment; (ii) the simple structured EWOD actuator facilitates a good concealment performance for two reasons: first, a further miniaturized and transparent microbot (0.07 g in weight and 1 cm in length) can be achieved, which promotes the optical concealment performance, and second, the aquatic TENG-Bot avoids reciprocating motions of the robot frame and restrains the heat and noise generation during operation, which improves the infrared and sonic concealment performance.

RESULTS AND DISCUSSION

Aquatic TENG-Bot and Actuation Mechanism. The concept image is illustrated in Figure 1. The aquatic TENG-Bot consists of one freestanding mode disc TENG, a floating part, and one EWOD actuator (EWA). The disc TENG is formed by an acrylic substrate, a pair of patterned copper

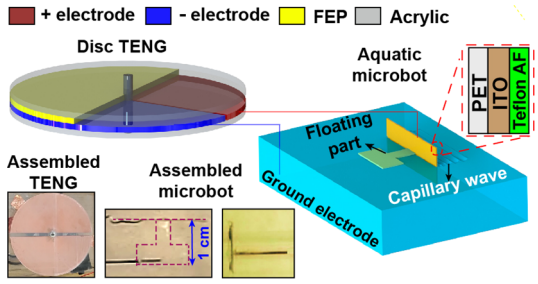

Figure 1. Concept of the aquatic TENG-Bot. The aquatic TENG-Bot is composed of a disc TENG and one EWA. During operation, the rotation of the disc TENG transfers charges to the actuator and ground electrodes alternatively and generates capillary waves for actuation.

electrodes, a commercial FEP (fluorinated ethylene and propylene) film, and an acrylic cover. The electrodes are thermally deposited to the acrylic substrate, and the commercial FEP film is stuck to the acrylic cover. The acrylic substrate is fixed and the electrodes are working as stator during operation. The acrylic cover is connected with the rod of a step motor and works as a rotor. The assembled disc TENG is shown in the inset of Figure 1. The EWA (2 cm in width and 0.8 cm in height) is stuck to the stern of the floating part. The top and side views of the assembled aquatic TENG-Bot are shown in the inset of Figure 1. The EWA is composed of a spin-coated and cured Teflon AF solution, a wet-etched ITO (indium tin oxide)-coated PET sheet, and connection wires. The transparent PET substrate and Teflon coating ensure optical concealment performance. The wet-etching of the ITO electrode is to prevent short-circuiting with water at the edge, and the cured Teflon thin film ensures a hydrophobic property on the actuator surface. The positive copper electrode of the disc TENG is connected with the actuator electrode (ITO) of the EWA, and the negative copper electrode of the disc TENG is inserted into water as a ground electrode. During operation, the FEP film rotates with the acrylic cover and alternatively contacts/separates with the positive/negative copper electrodes. The induced charge transfer modifies the surface energy of the actuator periodically and creates a capillary wave for actuation.

The working principle of the TENG-EWA is shown in Figure 2a. At stage <I>, the FEP film is in the middle of the negative and positive copper electrodes of the disc TENG. As the FEP film possesses excess negative charges on its surface, the same number of free electrons are pushed to the ground and actuator electrodes. The potential difference between the ground and actuator electrodes is zero, as shown in the V_{oc} plot at stage <I>; thus the water contact angle remains hydrophobic (contact angle: $\theta_{max} \approx 110°$). As the FEP film rotates to the negative copper electrode (stage <II>), the free electrons on the negative copper electrode are pushed to the ground electrode and a potential difference is established between ground and actuator electrodes. A contact angle reduction is induced by the EWOD phenomenon, and the modified contact angle can be expressed as

$$\theta_{min} = \cos^{-1}\left[\cos(\theta_{max}) + \frac{\varepsilon_0\varepsilon_r}{2\gamma_{LV}d}V_{eff}^{\ 2}\right] \quad (1)$$

in which ε_0 is the vacuum permittivity, ε_r is the relative permittivity of the Teflon AF layer, d is the Teflon AF layer

https://dx.doi.org/10.1021/acsnano.0c05901
ACS Nano 2020, 14, 15394−15402

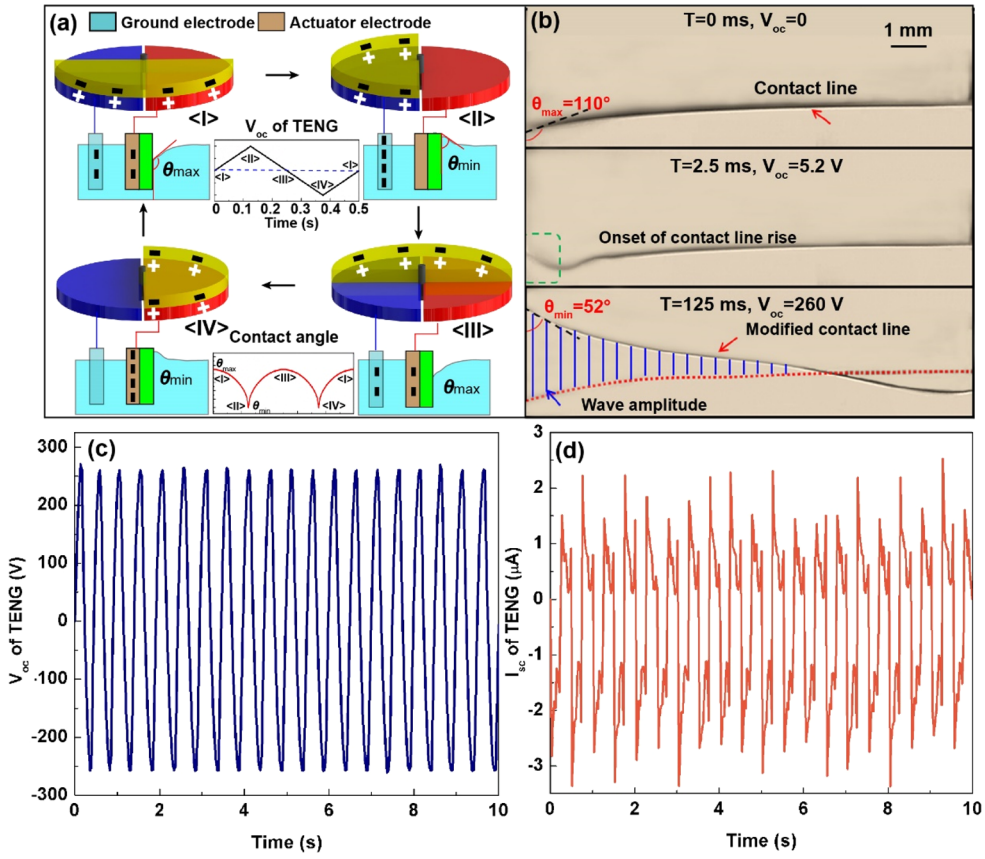

Figure 2. (a) Working mechanism of the TENG-EWA at different time steps. (b) Sequential snapshots of wave propagation induced by the TENG-EWA (V_{oc} = 520 V, f_{TENG} = 2 Hz, actuator electrode width w = 2 cm, Teflon AF thickness t = 1 μm). The green dashed square shows the onset of contact line rise at the moment of 2.5 ms. (c) Open-circuit voltage of the disc TENG. (d) Short-circuit current of the disc TENG.

thickness, γ_{LV} is the air−water interfacial tension, and V_{eff} is the effective potential difference between the ground and actuator electrodes, which is determined by the V_{oc} of disc TENG and actuator electrode width w. Once the contact angle is reduced, the contact line moves upward and a disturbance is induced at the air/water interface. When the FEP film rotates to the middle of the positive and negative copper electrodes again (stage <III>), the potential difference between ground and actuator electrodes vanishes. With the gravitational and capillary forces, the contact line recovers and the contact angle increases again. At stage <IV>, the free electrons are pushed to the actuator electrode and another potential difference is established, which leads to the second disturbance in water. If the FEP film keeps rotating along the disc TENG, a cycle from stage <I> to <IV> will be repeated. The disturbances in water form a capillary wave traversing against the actuator. The capillary wave exerts momentum to the actuator, and this is the origin of the actuation force. The variations of potential difference and contact angle of these stages could be found from the V_{oc} and contact angle plots.

A disc TENG with a diameter of 20 cm is assembled with one pair of positive and negative electrodes, and each electrode has a half-circle shape. The gap between the electrodes is 2 mm. A half-circle-shaped FEP film (20 cm in diameter and 50 μm in thickness) is stuck to the acrylic cover. The FEP film is driven by a step motor at a speed of 120 rpm, yielding a frequency (f_{TENG}) of 2 Hz in the output V_{oc} signal. The peak-to-peak open-circuit voltage of the disc TENG is ∼520 V (Figure 2c) and short-circuit current is ∼5 μA (Figure 2d). According to eq 1, the V_{oc} is the key effect that determines the actuation performance since the EWA possesses a comparable internal resistance to the TENG. It is noteworthy that this output performance is based on a commercial FEP film without any optimization. A larger open-circuit voltage or the same open-circuit voltage achieved by a much smaller TENG size can be expected with proper optimization methods on FEP. By connecting this voltage signal to an actuator with a width of 2 cm, a capillary wave is generated and captured by a high-speed camera at 2000 fps. The actuator is fixed to the side wall of an acrylic water container filled with DI water. As shown in Figure 2b, the contact line is in the middle of the air and water phases. At the moment of T = 0 ms, the V_{oc} is 0 and the initial contact angle is ∼110°. At the moment of T = 2.5 ms, the output voltage signal of the disc TENG applies to the actuator electrode and the onset of the contact line rise is observed. At the moment of T = 125 ms, the V_{oc} reaches a peak (260 V) and the contact angle reduces to the minimum value of ∼52°. The contact line rises to the highest point. From Figure 2b (T = 125 ms) the wave amplitude can be characterized by subtracting the highest contact line position by the initial contact line position. The captured high-speed video of the disc TENG induced capillary wave (one cycle, 0.5 s) could be found from Supplementary Movie 1. The propagation of the capillary wave agrees with the flow pattern of Stokes drift where a back-and-forth circle orbital can be observed.[24] The Stokes drift velocity can be represented by

https://dx.doi.org/10.1021/acsnano.0c05901
ACS Nano 2020, 14, 15394−15402

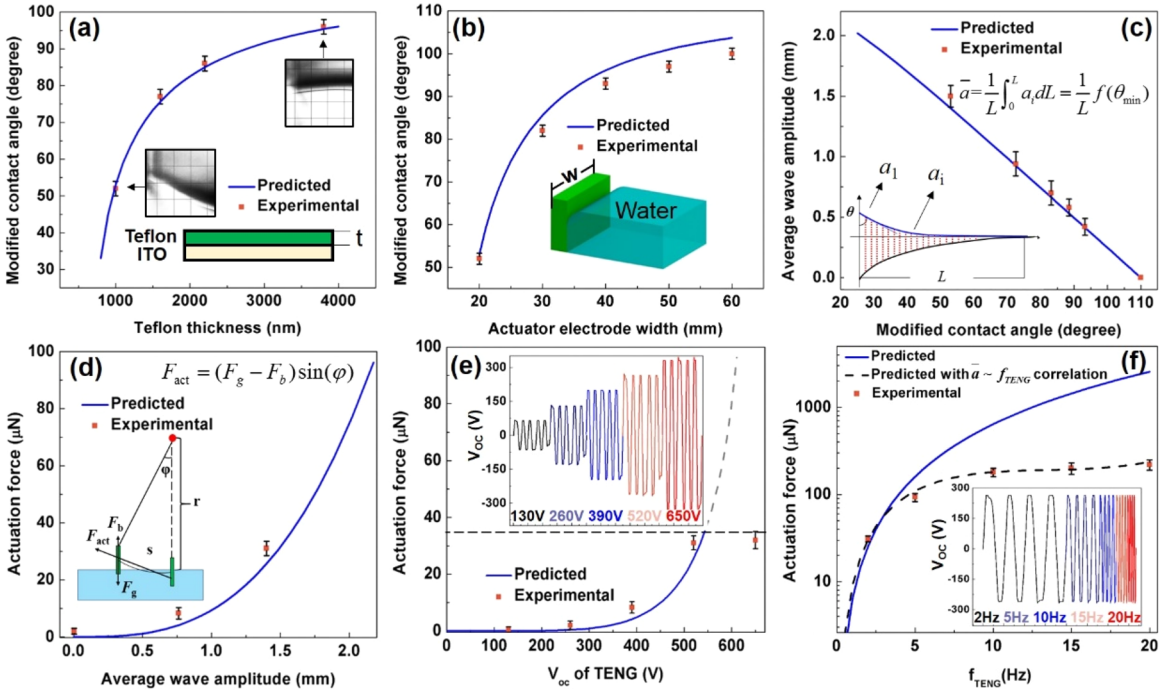

Figure 3. (a) Effect of Teflon layer thickness on the modified contact angle. (b) Effect of actuator electrode width on the modified contact angle. (c) Relationship between the modified contact angle and average wave amplitude. (d) Relationship between the actuation force and average wave amplitude. (e, f) Effects of V_{oc} and f_{TENG} on the actuation force.

$u_{drift} = k\omega a^2 e^{2kz}$, and this velocity is important for determining the actuation force of the TENG-EWA. In the equation, u_{drift} is the time-averaged drift velocity, k is the wavenumber, ω is the angular frequency, a is the amplitude of the capillary wave, and z is the vertical position from the free surface.

Performance of the TENG-CWA. The parameters affecting the performance of the actuators are varied to pursue the best actuation performance. The effect of Teflon AF layer thickness is firstly evaluated. In this test, the V_{oc}, f_{TENG}, and the actuator electrode width w are set as 520 V, 2 Hz, and 2 cm, respectively. The 10% Teflon AF solution was spin-coated with rotation speeds of 1000, 3000, 5000, and 7000 rpm, yielding thicknesses of 3.8, 2.2, 1.6, and 1 μm after curing. As shown in Figure 3a, the blue curve was obtained by eq 1, and the dots are measured by the high-speed camera captured image with the postprocessing software ImageJ. It is seen that the modified contact angle increases with the increase of Teflon thickness. This is due to the fact that the water contact line modulation on the actuator is achieved by electrostatic force which is inversely proportional to the distance (Teflon AF thickness) between the tribo-charges and the position to be measured. Another parameter determining the performance of the TENG-EWA is the actuator electrode width. In this test, the V_{oc}, f_{TENG}, and Teflon AF thickness t are kept as 520 V, 2 Hz, and 1 μm. As shown in Figure 3b, with the increase of the actuator electrode width, the modified contact angle increases. This is because when the disc TENG output is fixed, the total amount of tribo-charges transferred to the actuator electrodes would be the same. An increase in the actuator electrode width leads to a reduced charge density on the Teflon AF layer and less contact line modulation. To model the effect of the actuator electrode width w, an effective voltage is defined as $V_{eff} = V_{oc}/(pw)$. In which p is a constant with a unit of 1/m and the value from curve fitting is 291. A detailed relationship between V_{oc} and V_{eff} can be found in Figure S1 in the Supporting Information.

In order to quantify the actuation force of the TENG-EWA, the average wave amplitude $\bar{a}$ is important, and the relationship between the modified contact angle and $\bar{a}$ is derived. As shown in the inset of Figure 3c, when the contact angle is modified by the tribo-charges from disc TENG, the wave amplitude could be attained by subtracting the modified contact line from the initial contact line. The average wave amplitude can be estimated as

$$\bar{a} = \frac{\int_0^L a_i dL}{L} \approx \frac{f(\theta_{min})}{L} \quad (2)$$

where L is the length that the capillary wave propagates and a_i is an infinitesimal wave amplitude. $f(\theta_{min})$ is a function of modified contact angle, and the complete expression can be found from the Supporting Information. It is seen from Figure 3c that the average wave amplitude drops linearly with the increase of the modified contact angle θ_{min}. With the momentum theorem, an actuation force model is presented in eq 3.

$$F_{act} = \frac{mu_{drift}}{\Delta t} \quad (3)$$

where Δt is the duration of the applied actuation force and m is the mass of water that is disturbed. This mass can be estimated by the wave propagation length L, average wave amplitude $\bar{a}$, actuator electrode width w, and the density of water ρ. The drift velocity at the free surface ($z = 0$) can be expressed as $u_{drift} = k\omega a^2$. The wavenumber k can be estimated by the gravity–capillary wave dispersion relation.[25] As the contact angle varies with the square of the V_{oc} signal (eq 1), there exist two peaks in wave oscillation during one cycle of the V_{oc} signal. The wave angular frequency could be represented by $\omega = 4\pi f_{TENG}$. The

https://dx.doi.org/10.1021/acsnano.0c05901
ACS Nano 2020, 14, 15394−15402

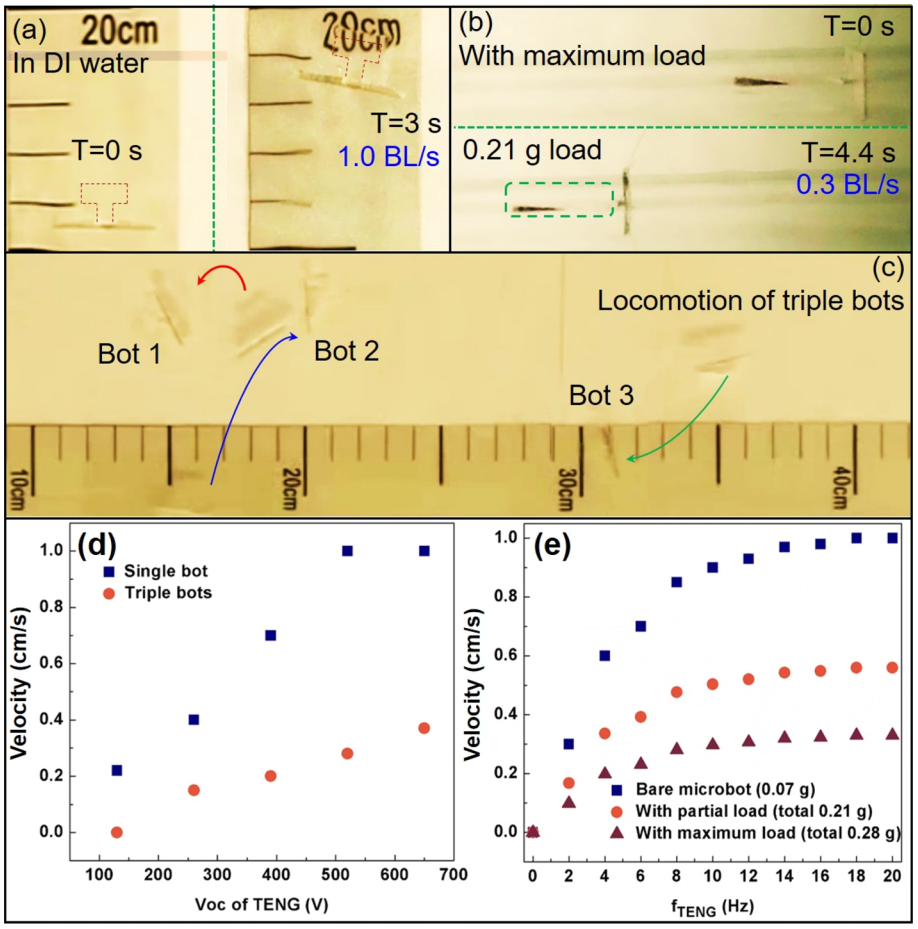

Figure 4. Locomotion of the aquatic TENG-Bot in DI water. (a) Locomotion of single bot in DI water at a maximum velocity of 1 cm/s. (b) Locomotion of the microbot with a maximum load (three times the bare microbot) in DI water. (c) Locomotion of triple bots in DI water. (d) Effects of V_{oc} of the TENG on the locomotion velocity. (e) Effects of f_{TENG} and load weight on the locomotion velocity.

disturbed water (with a mass of m) is assumed to oscillate at an average wave amplitude $\bar{a}$. Now the actuation force can be represented by eq 4, and the relationship between the actuation force (F_{act}) and the affecting parameters V_{oc}, f_{TENG}, θ_{max}, θ_{min}, w, and t can be analyzed:

$$F_{act} = 16\pi^2 {f_{TENG}}^2 wL\rho k(\bar{a})^3 \quad (4)$$

From eq 4, the actuation force F_{act} is found to be proportional to the third power of the average wave amplitude, and an agreement between the model prediction and experimental results is achieved as shown in Figure 3d. The inset of Figure 3d presents the schematic of force measurement by an optical method with force balance. The details of the actuation force measurement could be found from Figure S5 in the Supporting Information.

Substituting eqs 1 and 2, the expression of effective voltage V_{eff}, and the expression of Stokes drift velocity at the free surface into eq 4, the relationship between the actuation force and V_{oc} of the disc TENG can be established. To verify this relationship, diverse sizes of TENGs with diameters of 10, 14, 17.5, 20, and 22.5 cm were prepared and yielded V_{oc} values of ~130, 260, 390, 520, and 650 V. An actuator with a width w of 2 cm and Teflon AF thickness of 1 μm was used for the test. The frequency was set as 2 Hz. For the disc TENGs with V_{oc} between 130 and 520 V, the actuation forces agree well with the theoretical prediction as shown in Figure 3e. When the V_{oc} increases to 650 V, the measured actuation force deviates from the predicted value, and this is due to the contact angle saturation. As shown in eq 4, the actuation force is proportional to the square of the disc TENG frequency. However, the experimental data deviate from the model when the frequency exceeds 5 Hz. This is mainly due to the fact that the average wave amplitude decreases when the frequency increases. As presented in the Supplementary Movie 1, the contact line receding process takes longer (175 ms) as compared to the advancing process (75 ms). Such a long receding duration is not enough for the contact line to return to the initial hydrophobic position when the frequency increases. The contact line oscillates in a narrower contact angle range and leads to the reduction of the average wave amplitude. The relationship of the average wave amplitude is measured at various frequencies (Figure S6 in Supporting Information), and the curve fitting relationship between average wave amplitude and frequency is substituted into eq 4. As shown by the dashed line in Figure 3f, the predicted actuation force with the frequency-dependent wave amplitude matches the measured actuation force well.

Locomotion of the Aquatic TENG-Bot. In this section, the locomotion of the aquatic TENG-Bot in DI water is firstly presented. The V_{oc} and f_{TENG} are varied to show their effects on the locomotion velocity. Figure 4a shows a single microbot's (0.07 g in weight) locomotion in a container filled with DI water. The actuation electrode was connected to the

https://dx.doi.org/10.1021/acsnano.0c05901
ACS Nano 2020, 14, 15394−15402

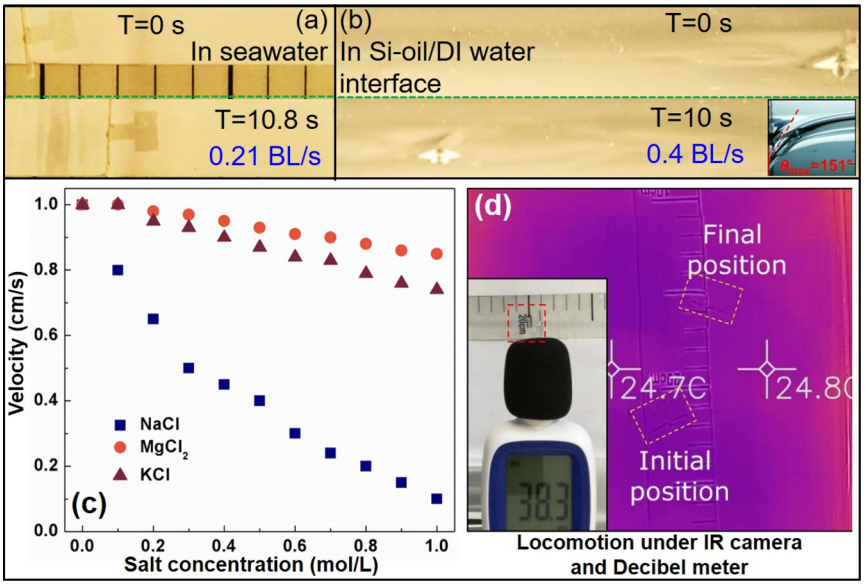

Figure 5. Locomotion of the aquatic TENG-Bot in diverse working environments. (a) Locomotion in seawater (collected from Heishijiao Park, 121.565677 E, 38.875297 N, Dalian, China) at a velocity of 0.21 cm/s. (b) Locomotion of the microbot at the silicone-oil/DI water interface at a velocity of 0.4 cm/s. (c) Effects of ion type and concentration on the locomotion velocity. (d) Locomotion under an IR camera and decibel meter. The red dashed square represents the location of the microbot under the noise test, and the yellow dashed squares represent the initial and final positions of the microbot under the IR camera test.

TENG with a 25 μm nickel wire for reducing the strain. By switching on the disc TENG, a 520 V and 20 Hz output signal is generated, and the bare microbot was actuated forward at a maximum locomotion velocity of 1 cm/s (~1 BL/s). Details of the microbot actuation can be found in Figure 4a and Supplementary Movie 2. The effects of the V_{oc} on the single microbot locomotion are presented in Figure 4d (f_{TENG} kept as 20 Hz). It is seen that a single aquatic TENG-Bot can be actuated when the V_{oc} is ~130 V at a velocity of 0.2 cm/s. The locomotion velocity saturates when the V_{oc} reaches 520 V, and this result agrees with the trend of actuation force as shown in Figure 3e. The 520 V and 20 Hz TENG output signal is further employed for the locomotion of triple bots simultaneously. As shown in Figure 4c, the three microbots move at an average velocity of ~0.3 cm/s (Supplementary Movie 3). The effects of V_{oc} on the triple bots' locomotion are shown in Figure 4d. It is seen that the locomotion velocity of the triple bots is much lower than the single bot. This is due to the reduction in transferred charge density on each actuator and the decreased wave amplitude which is responsible for actuation force. The locomotion performance of the aquatic TENG-Bot with partial and maximum loads is shown in Figure 4b and e. In Figure 4b, a load made from commercial copper tape with a weight of 0.21 g (three times the net bot's weight) is stuck to the floating part of the aquatic TENG-Bot. The velocity decreases to ~0.29 cm/s at the TENG output of 520 V and 20 Hz (Supplementary Movie 4), and the reduction in velocity is due to the increased drag force induced by the larger contact area when loads are applied. As shown in Figure 4e, the increase of load weight reduces the locomotion velocity. The increase in the f_{TENG} from 2 to 5 Hz promotes the velocity significantly. The locomotion velocity saturates when the frequency further increases above 10 Hz, which agrees well with the actuation force trend in Figure 3f.

The locomotion function of the presented aquatic TENG-Bot is also demonstrated in seawater, as shown in Figure 5a and Supplementary Movie 5. The output of the TENG is kept as 520 V and 20 Hz. The seawater was collected from the coast of Heishijiao Park (121.565677E, 38.875297N) in Dalian, China. The seawater was used as collected. The salt concentration is ~30 wt %, and a locomotion velocity of 0.21 cm/s was achieved. The decreased locomotion velocity in seawater is due to the ions' induced wave amplitude reduction. When salts are added to the DI water, the electrical conductivity of the solution increases due to the large number of freely moving ions in the water, and the electrical conductivity of the solution increases with the concentration of the added salt. The freely moving ions would be easily attracted by the transferred tribo-charges. On the contrary, this part of the compensated tribo-charges contributes less to the electrostatic force for modifying the water contact line. In order to quantify the effects of different ions, the locomotion performance of the aquatic TENG-Bot in salt water was further tested. As shown in Figure 5c, the addition of three types of salts including NaCl, $MgCl_2$, and KCl with concentrations of 0−1 mol/L causes an adverse effect on the microbot's locomotion. When 1 mol/L NaCl was added to DI water, the locomotion velocity drops to around 0.1 cm/s. In 1 mol/L KCl and $MgCl_2$ solution, the aquatic microbot moves at a velocity of 0.8 and 0.9 cm/s. The difference induced by salt type could be attributed to the electronegativity of ions as well as the contact angle variation when ions exist. A low-electronegativity cation is preferred to adsorb F^- groups on the Teflon AF surface.[26] The electronegativities of the cations Na^+, K^+, and Mg^{2+} are 0.9, 0.82, and 1.16, indicating that Mg^{2+} is the least preferred to adsorb F^- groups on Teflon, thus yielding the least reduction in the locomotion velocity. The electronegativities of Na^+ and K^+ are comparable, and the reason for the most reduction of locomotion velocity in NaCl could be attributed to a slight reduction of contact angle of the high-concentration NaCl solution on a hydrophobic surface.[27] A reduced initial contact angle narrows down the maximum range of contact line modulation, thus generating a weaker actuation force. The performance of the aquatic microbot at

https://dx.doi.org/10.1021/acsnano.0c05901
ACS Nano 2020, 14, 15394−15402

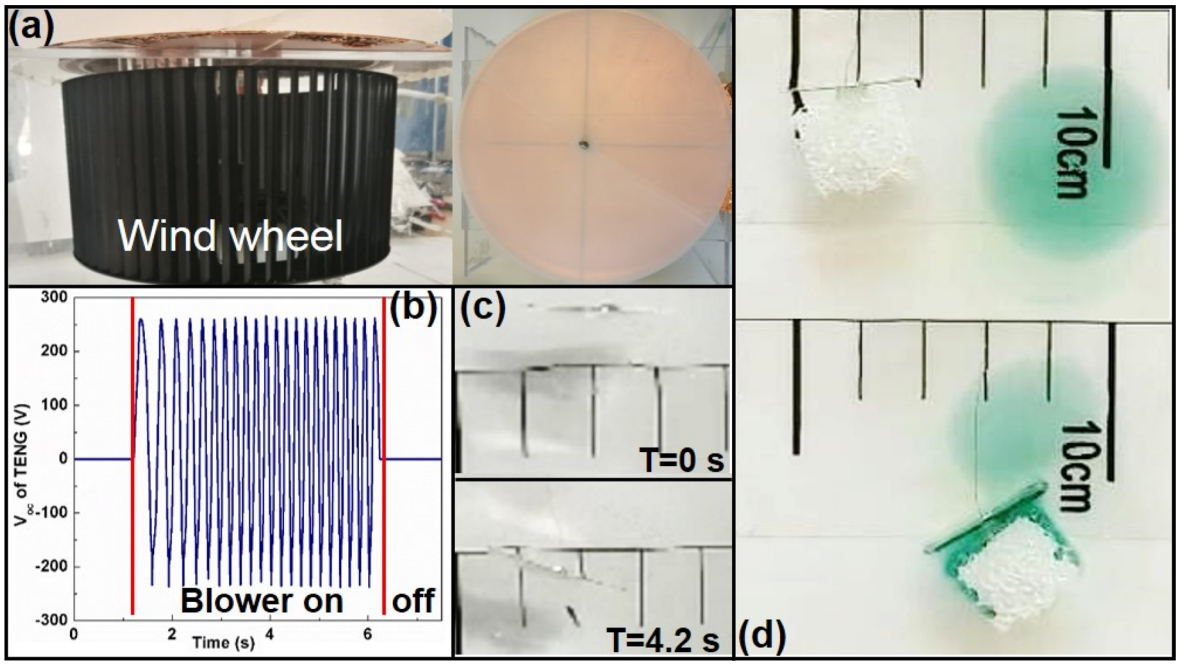

Figure 6. Wind-TENG actuated microbot and the application for oil drop collection. (a) The wind-TENG device is composed of a wind wheel and a TENG with two pairs of electrodes. (b) The wind wheel is driven by a blower with a wind speed of 0.25 m/s and generates a V_{oc} of 500 V at a frequency of 4.2 Hz. (c) The aquatic TENG-Bot was actuated against the wind at a speed of 0.29 cm/s. (d) The aquatic TENG-Bot was equipped with a hydrophobic but oleophilic sponge and demonstrated the collection of an ink-dyed oil drop on the water surface.

the silicone-oil and DI water interface was further evaluated. When replacing the air phase by 5 cst silicone oil (5 mm in height), the initial water contact angle θ_{max} increases to 151°; this is due to the increased silicone-oil/actuator wall interfacial tension. The increased initial contact angle facilitates the generation of a much larger average wave amplitude. An average wave amplitude of 3.5 mm was measured at the silicone-oil/DI water interface, which is much larger than the value of 1.5 mm for the DI water/air case. However, the existence of silicone oil increases the resistance of the microbot, thus yielding a locomotion velocity of 0.4 cm/s when the output of the TENG is 520 V and 20 Hz. Details of the locomotion at the silicone-oil/DI water interface can be found in Figure 5b and Supplementary Movie 6. The wave propagations of two fixed TENG-EWAs at air/DI water and silicone-oil/DI water interfaces are captured by a CCD camera and can be found in Supplementary Movie 7.

With the transparent robot frame and small size, the aquatic TENG-Bot was camouflaged well optically (as shown in Figure 4a–c). In order to evaluate the infrared and sonic concealment performance, the aquatic TENG-Bot was further tested under infrared camera and a decibel meter. As shown in Figure 5d, the TENG-Bot moves 5 body lengths from the initial position to the final position, and the whole locomotion process could not be detected by the IR camera, as shown in the Supplementary Movie 8. Besides, the actuation of the aquatic TENG-Bot is quiet, and the decibel meter only collected environmental noise of ~38 dB (Supplementary Movie 9). The good infrared concealment performance could be attributed to the large internal resistances of both the TENG and EWA, which induce a tiny current flow and undetectable heat generation. Besides, the actuation mode of EWA is free of reciprocating motion of the robot frame, which leads to less heat and noise production.

Wind-TENG-Driven Aquatic TENG-Bot and Application. In this section, a wind-TENG is assembled for harvesting the environmental wind energy for the actuation of the aquatic TENG-Bot (Figure 6a). The wind-TENG is designed with two pairs of electrodes to increase the frequency of the output signal at low wind speed conditions. When a 0.25 m/s wind is blown on the blade, the TENG could generate a peak-to-peak voltage signal of ~500 V with a frequency of 4.2 Hz (Figure 6b). The aquatic TENG-Bot is actuated forward at a speed of 0.29 cm/s against the wind (Figure 6c and Supplementary Movie 10).

CONCLUSIONS AND FUTURE PERSPECTIVES

This work presents a TENG-enabled EWOD actuator for aquatic microbots. With the simple device structure, an ultralightweight and optical transparent aquatic TENG-Bot of only 0.07 g is actuated at a maximum speed of 1 BL/s. The weight of the presented aquatic TENG-Bot is only heavier than the water strider (*Gerridae*). The actuation of the EWA is free of moving parts with tiny heat and noise generation. These features endow the aquatic TENG-Bot with good optical, infrared, and sonic concealment performance. This work not only demonstrates the environmental wind energy actuated microbots, but also shows the potential for the application with concealment requirements. It is noteworthy that the current TENG device is much heavier than the microbot, which limits the advantage provided by the lightweight microbot. With the further development of TENG technology, lightweight TENG devices with large-amplitude and high-frequency output can be expected, and the aquatic TENG-Bot could be driven in an untethered and self-powered way.

METHODS

Device Fabrication. The electrodes of the disc TENG were assembled by thermally depositing copper onto a patterned acrylic

https://dx.doi.org/10.1021/acsnano.0c05901
ACS Nano 2020, 14, 15394–15402

substrate at a deposition rate of 0.8 nm/s. Commercial FEP film with a thickness of 50 μm is tailored with the same size of the copper electrode and stuck to the acrylic cover by double-sided tape. The two terminals of the disc TENG were connected to the ground and actuator electrodes by nickel wires with a diameter of 25 μm; such a thin connecting wire is to reduce the wire-induced strain on the aquatic TENG-Bot. The acrylic cover with FEP film was driven by a step motor. The output signal frequency could be tuned by adjusting the rotation speed controller. The ground electrode is a bare copper wire with a clip, which is directly inserted into the water. The actuator electrode is made of an ITO-coated PET sheet with a thickness of 175 μm; 1 mm of the ITO electrode at the edges was etched away to avoid a short-circuit with water. The size of the actuator electrode is 0.8 cm × 2 cm. A 10% Teflon AF solution was prepared by dissolving the AF 1600× powder in an FC-40 solution at 60 °C for 48 h. The prepared Teflon AF solution was spin coated on the prepared actuator electrode at speeds of 1000, 3000, 5000, and 7000 rpm, yielding Teflon layer thicknesses of 3.8, 2.2, 1.6, and 1 μm. The spin-coated actuator electrode was dried and cured in a convection oven at 80 °C (avoiding mechanical deformation of the PET substrate) for 5 h. The floating part of the aquatic TENG-Bot was obtained by tailoring a PET sheet into a polygon as shown in Figure 1 with a long edge of 1 cm and short edge of 0.5 cm. The floating part was stuck to the back center of the prepared actuator. The experiment was conducted in an acrylic box (20 cm × 20 cm × 10 cm), filled with DI water (electrical resistivity >1 MΩ·cm) with a depth of 2 cm. In the locomotion performance test, the seawater was collected from a local park in Dalian city, and the seawater was used as collected without any treatment. The 5 cst silicone oil was poured into a container filled with DI water to test the locomotion of the TENG-Bot at the silicone-oil/DI water interface.

Characterization. The output signal of the disc TENG was recorded by a Keithley 6514 electrometer. The wave property was recorded by a high-speed camera (Photron Mini UX50) at 2000 frames per second. A calibration ruler was placed at the focal plane of the camera to quantify the wave amplitude. A commercial superhydrophobic coating (Neverwet) was applied to the calibration ruler to reduce its influence on wave propagation. The actuation force is characterized by an optical method with moment equilibrium. Details of the force measurement setup can be found in the Supporting Information.

ASSOCIATED CONTENT

Supporting Information

The Supporting Information is available free of charge at https://pubs.acs.org/doi/10.1021/acsnano.0c05901.

Capillary wave propagation (AVI)

Locomotion in DI water at maximum velocity (AVI)

Locomotion of triple bots (AVI)

Locomotion with maximum load (AVI)

Locomotion in seawater (AVI)

Locomotion at the silicone oil and DI water interface (AVI)

Comparison of wave propagation at water−air and water−oil interfaces (AVI)

Locomotion under IR camera (AVI)

Locomotion under a decibel meter (AVI)

Wind-TENG-driven aquatic microbot (AVI)

Relationship between the effective voltage applied to the EWOD actuator and the open-circuit voltage of the TENG; derivation of the relationship between average wave amplitude and modified contact angle; measurement principle of actuation force; relationship between the average wave amplitude and frequency (PDF)

AUTHOR INFORMATION

Corresponding Authors

Dongyue Jiang − *Key Laboratory of Ocean Energy Utilization and Energy Conservation of Ministry of Education, Dalian University of Technology, Dalian, China 116024*; orcid.org/0000-0002-4277-451X; Email: jiangdy@dlut.edu.cn

Minyi Xu − *Marine Engineering College, Dalian Maritime University, Dalian, Liaoning, China 116026*; Email: xuminyi@dlmu.edu.cn

Zhong Lin Wang − *Beijing Institute of Nanoenergy and Nanosystems, Chinese Academy of Sciences, Beijing, China 100083; School of Materials Science and Engineering, Georgia Institute of Technology, Atlanta, Georgia 30332, United States*; orcid.org/0000-0002-5530-0380; Email: zhong.wang@mse.gatech.edu

Authors

Zeng Fan − *School of Physics, Dalian University of Technology, Dalian, China 116024*

Hongchen Wang − *Key Laboratory of Ocean Energy Utilization and Energy Conservation of Ministry of Education, Dalian University of Technology, Dalian, China 116024*

Guijun Chen − *Key Laboratory of Ocean Energy Utilization and Energy Conservation of Ministry of Education, Dalian University of Technology, Dalian, China 116024*

Yongchen Song − *Key Laboratory of Ocean Energy Utilization and Energy Conservation of Ministry of Education, Dalian University of Technology, Dalian, China 116024*

Complete contact information is available at: https://pubs.acs.org/10.1021/acsnano.0c05901

Notes

The authors declare no competing financial interest.

ACKNOWLEDGMENTS

This work was supported by National Natural Science Foundation of China (51906031, 51803018, 51879022) and Fundamental Research Funds for the Central Universities, DUT20LAB105. We thank Prof. J. Tian and Prof. Z. Lei from Dalian University of Technology for effective discussions on high-speed imaging and actuation force measurement.

REFERENCES

(1) Jadaliha, M.; Choi, J. Environmental Monitoring Using Autonomous Aquatic Robots: Sampling Algorithms and Experiments. *IEEE Trans. Control Syst. Technol.* **2013**, *21*, 899−905.

(2) Torres-Méndez, L. A.; Dudek, G. Color Correction of Underwater Images for Aquatic Robot Inspection. *'EMMCVPR'05 Proceedings of the 5th International Conference on Energy Minimization Methods in Computer Vision and Pattern Recognition* **2005**, *3757*, 60−73.

(3) Chen, Y.; Doshi, N.; Goldberg, B.; Wang, H.; Wood, R. J. Controllable Water Surface to Underwater Transition Through Electrowetting in a Hybrid Terrestrial-Aquatic Microrobot. *Nat. Commun.* **2018**, *9*, 2495.

(4) Becker, F.; Zimmermann, K.; Volkova, T.; Minchenya, V. T. An Amphibious Vibration-Driven Microrobot with a Piezoelectric Actuator. *Regul. Chaotic Dyn.* **2013**, *18*, 63−74.

(5) Godaba, H.; Li, J.; Wang, Y.; Zhu, J. A Soft Jellyfish Robot Driven by a Dielectric Elastomer Actuator. *IEEE Robot. Autom. Lett.* **2016**, *1*, 624−631.

(6) Yuk, H.; Lin, S.; Ma, C.; Takaffoli, M.; Fang, N. X.; Zhao, X. Hydraulic Hydrogel Actuators and Robots Optically and Sonically Camouflaged in Water. *Nat. Commun.* **2017**, *8*, 14230.
(7) Zhang, X.; Zhao, J.; Zhu, Q.; Chen, N.; Zhang, M.; Pan, Q. Bioinspired Aquatic Microrobot Capable of Walking on Water Surface Like a Water Strider. *ACS Appl. Mater. Interfaces* **2011**, *3*, 2630−6.
(8) Chen, Y.; Wang, H.; Helbling, E. F.; Jafferis, N. T.; Zufferey, R.; Ong, A.; Ma, K.; Gravish, N.; Chirarattananon, P.; Kovac, M. A Biologically Inspired, Flapping-Wing, Hybrid Aerial-Aquatic Microrobot. *Sci. Robot.* **2017**, *2*, No. eaao5619.
(9) Ji, X.; Liu, X.; Cacucciolo, V.; Imboden, M.; Shea, H. An Autonomous Untethered Fast Soft Robotic Insect Driven by Low-Voltage Dielectric Elastomer Actuators. *Sci. Robot.* **2019**, *4*, No. eaaz6451.
(10) Ma, K. Y.; Chirarattananon, P.; Fuller, S. B.; Wood, R. J. Controlled Flight of a Biologically Inspired, Insect-Scale Robot. *Science* **2013**, *340*, 603−607.
(11) Hu, D. L.; Chan, B.; Bush, J. W. M. The Hydrodynamics of Water Strider Locomotion. *Nature* **2003**, *424*, 663−666.
(12) Fan, F.-R.; Tian, Z.-Q.; Wang, Z. L. Flexible Triboelectric Generator. *Nano Energy* **2012**, *1*, 328−334.
(13) Wang, Z. L. Triboelectric Nanogenerators as New Energy Technology for Self-Powered Systems and as Active Mechanical and Chemical Sensors. *ACS Nano* **2013**, *7*, 9533−9557.
(14) Fan, F.-R.; Lin, L.; Zhu, G.; Wu, W.; Zhang, R.; Wang, Z. L. Transparent Triboelectric Nanogenerators and Self-powered Pressure Sensors Based on Micropatterned Plastic Films. *Nano Lett.* **2012**, *12*, 3109−3114.
(15) Wang, Z. L. On Maxwell's Displacement Current for Energy and Sensors: the Origin of Nanogenerators. *Mater. Today* **2017**, *20*, 74−82.
(16) Wang, Z. L.; Wang, A. C. On the Origin of Contact-Electrification. *Mater. Today* **2019**, *30*, 34−51.
(17) Kwak, S. S.; Kim, S. M.; Ryu, H.; Kim, J.; Khan, U.; Yoon, H.-J.; Jeong, Y. H.; Kim, S.-W. Butylated Melamine Formaldehyde as a Durable and Highly Positive Friction Layer for Stable, High Output Triboelectric Nanogenerators. *Energy Environ. Sci.* **2019**, *12*, 3156−3163.
(18) Wang, H.; Xu, L.; Bai, Y.; Wang, Z. L. Pumping Up the Charge Density of a Triboelectric Nanogenerator by Charge-Shuttling. *Nat. Commun.* **2020**, *11*, 4203.
(19) Kim, J.; Ryu, H.; Lee, J. H.; Khan, U.; Kwak, S. S.; Yoon, H.-J.; Kim, S.-W. High Permittivity $CaCu_3Ti_4O_{12}$ Particle-Induced Internal Polarization Amplification for High Performance Triboelectric Nanogenerators. *Adv. Energy Mater.* **2020**, *10*, 1903524.
(20) Hinchet, R.; Yoon, H.-J.; Ryu, H.; Kim, M.-K.; Choi, E.-K.; Kim, D.-S.; Kim, S.-W. Transcutaneous Ultrasound Energy Harvesting Using Capacitive Triboelectric Technology. *Science* **2019**, *365*, 491−494.
(21) Chen, G.; Liu, X.; Li, S.; Dong, M.; Jiang, D. A Droplet Energy Harvesting and Actuation System for Self-powered Digital Microfluidics. *Lab Chip* **2018**, *18*, 1026−1034.
(22) Yuan, J.; Cho, S. K. Mechanism and Flow Measurement of AC Electrowetting Propulsion on Free Surface. *Exp. Fluids* **2015**, *56*, 67.
(23) Chung, S. K.; Ryu, K.; Cho, S. K. Electrowetting Propulsion of Water-Floating Objects. *Appl. Phys. Lett.* **2009**, *95*, 014107.
(24) Mesquita, O. N.; Kane, S.; Gollub, J. P. Transport by Capillary Waves: Fluctuating Stokes Drift. *Phys. Rev. A: At., Mol., Opt. Phys.* **1992**, *45*, 3700−3705.
(25) Billingham, J.; King, A. C. Nonlinear Water Waves, Wave Motion. *Cambridge Texts in Applied Mathematics*; Cambridge University Press: Cambridge, 2001; pp 269−307.
(26) Pan, L.; Wang, J.; Wang, P.; Gao, R.; Wang, Y.-C.; Zhang, X.; Zou, J.-J.; Wang, Z. L. Liquid-FEP-Based U-Tube Triboelectric Nanogenerator for Harvesting Water-Wave Energy. *Nano Res.* **2018**, *11*, 4062−4073.
(27) Sghaier, N.; Prat, M.; Ben Nasrallah, S. On the Influence of Sodium Chloride Concentration on Equilibrium Contact Angle. *Chem. Eng. J.* **2006**, *122*, 47−53.

https://dx.doi.org/10.1021/acsnano.0c05901
ACS Nano 2020, 14, 15394−15402